Tethered DNA dynamics in shear flow

Yu Zhang,[1] Aleksandar Donev,[2] Todd Weisgraber,[2] Berni J. Alder,[2] Michael D. Graham,[1] and Juan J. de Pablo[1,*]

[1]*Department of Chemical and Biological Engineering, University of Wisconsin-Madison, Madison, WI 53706-1691*

[2]*Lawrence Livermore National Laboratory, P.O.Box 808, Livermore, CA 94551-9900*

(Dated: May 5, 2009)

Abstract

We study the cyclic dynamics of a single polymer tethered to a hard wall in shear flow using Brownian Dynamics, the Lattice Boltzmann Method, and a recent Stochastic Event-Driven Molecular Dynamics (SEDMD) algorithm. We focus on the dynamics of the free end (last bead) of the tethered chain and we examine the cross-correlation function (CCF) and power spectral density (PSD) of the chain extensions in the flow and gradient directions as a function of chain length N and dimensionless shear rate Wi. Extensive simulation results suggest a classical fluctuation-dissipation stochastic process and question the existence of periodicity of the cyclic dynamics, as previously claimed. We support our numerical findings with a simple analytical calculation for a harmonic dimer in shear flow.

I. INTRODUCTION

The interaction of polymer molecules with fluid flow has been studied both theoretically[1,2] and experimentally[3–7] for several decades. The behavior of polymer chains in flow is determined by an intricate interplay between the flow gradients, chain elasticity, thermal fluctuations, and the physical confinement[8,9]. The dynamics of tethered polymer molecules ("polymer brushes") in shear flow has received considerable attention due to its relevance to diverse important applications, such as colloidal stabilization, surface adhesion, and lubrication[10].

In contrast to previous work on the collective motion of polymer brushes[10,11], Doyle *et al.* studied the dynamics of a single tethered DNA in uniform shear flow using fluorescence videomicroscopy[12]. Enhanced temporal fluctuations in the chain extension were observed, and were attributed to the coupling of advection in the flow direction and diffusion in the gradient direction. A cyclic dynamics mechanism (Fig.1), closely related to the tumbling dynamics of a free polymer molecule in shear flow[7,13,14], was proposed based on results from Brownian dynamics simulations. No peaks were observed in the calculated power spectral density (PSD) of the DNA extension in the flow direction, and the authors therefore suggested that the cyclic dynamics of a tethered chain in shear flow is aperiodic. An important physical question is whether there is a characteristic timescale associated with the cyclic motion that is distinct from the internal relaxation time of the chain.

Several computational studies revisited the problem of a tethered chain in shear flow by looking at different variables relating to both the flow and gradient directions, such as extensions along both flow and gradient directions[15], polymer orientation angle defined through the gyration tensor[14], and angle between the wall and the vector joining the tethering point to the center-of-mass of the chain[16]. The cross-correlation functions for such variables exhibit signatures of the proposed cyclic motion in the form of peaks at non-zero delay time. Because of the particular choice of variables in Ref. [16], the lack of such peaks at small Weissenberg numbers was attributed to the existence of a critical Weissenberg number; as demonstrated in Ref. [17], choosing a different sets of variables shows that the signature peaks exist even at small shear rates. In Ref. [16], the position of the peak in the studied cross-correlation functions was interpreted as a characteristic cycling time, and it was found to be a fraction of the relaxation time of the polymer chain. In Ref. [14] the tumbling motion of a free polymer chain in shear flow was studied experimentally and computationally, and

wide peaks were found in the Fourier spectra of the time series of the angle of the chain relative to the flow direction. These peaks were identified as evidence of periodic motion of the tumbling molecule. The characteristic tumbling time (period) was extracted from the position of the peak in the spectrum and was found to be in good agreement with the experimentally-measured tumbling frequency. These finding for a free chain in shear flow inspired similar studies of a tethered chain, and similar observations of periodic motion with a characteristic period about an order of magnitude larger than the relaxation time were reported[14,15,18]. In several later studies of the tumbling emotion of a free polymer chain in shear flow, experimental results[7], numerical simulation[13], and theory[19,20] all suggest that the intervals between successive tumbling events are exponentially-distributed with a decay constant equal to the relaxation time of the chain. Such an exponential tail implies that the tumbling events occur as a Poisson-like process, which is aperiodic despite the existence of a characteristic timescale (frequency of repetition). If the tumbling events of a free polymer in shear flow is aperiodic, intuitively, adding of a wall to break the symmetry of the motion should leave the dynamics of a tethered chain aperiodic.

Different authors use the terms "cyclic" (repetitive) and "periodic" with different meanings, and it is therefore important to give our definitions. Periodicity is the quality of occurring in regular time intervals (periods). Periodic motion has correlation functions that are (possibly damped) oscillatory functions, and spectra that have sharp peaks. Noise (fluctuations) and the associated dissipation will always broaden any peaks that are related to underlying deterministic periodic motion (and consequently, exponentially dampen the oscillations in the real-space correlation functions). As an example, for a rigid spheroid in shear flow, there is indeed periodic motion (Jeffery's orbits) in pure shear flow. Adding fluctuations, when they are small, is expected to preserve that but introduce some broadening of the spectral peaks[21]. In contrast, a cycle usually means a process that eventually returns to its beginning and then repeats itself in the same sequence. The end-to-end tumbling of a single polymer molecule in shear flow provides a relevant example. In this paper we analytically calculate the power spectrum for a tethered dimer in shear flow, and find an exponentially-decaying cross-correlation function that has the relaxation time as the only characteristic timescale. More importantly, this analytical example shows that the power spectrum can exhibit a wide peak at small frequencies without any underlying periodic motion, and that the location of a maximum in the PSD is not necessarily an indication of a

new timescale. The analytical results for a tethered dimer are consistent with our numerical observations for longer tethered chains in shear flow. Therefore, our investigations do not confirm the existence of periodic motion with a period distinct from the relaxation time of the chain, as previously suggested in the literature[14,15,18].

We apply three different solvent representations to the same problem of a tethered chain in shear flow. The models are an implicit solvent (Brownian Dynamics[22], BD), a continuum solvent (Lattice-Boltzmann[23], LB), and a particle solvent (Direct Simulation Monte Carlo[17], DSMC). Such comparison between widely differing methods on the *same problem* is important as a validation of their range of applicability. It is also important to compare the computational performance of the different methods. In this work, different chain representations and boundary conditions make a direct quantitative comparison impossible. Specifically, the BD polymer is a worm-like chain representative of semi-flexible DNA, in the LB simulations it is a flexible chain of repulsive spheres, and in the DSMC solvent it is a flexible chain of hard spheres. However, we can access the importance of the details of the chain model, and in particular, of chain elasticity, and thus test the widely used assumption that the dynamics scales with the Weissenberg number $Wi = \dot{\gamma}\tau$, where $\dot{\gamma}$ is the shear rate and τ the chain relaxation time, independent of the details of the model. For this particular problem of a tethered chain in shear flow, we find good agreement between the different methods.

A general discussion of the wide range of techniques for modeling the hydrodynamics of polymer chains in solution is given in Section II. Further details about the three specific techniques we use in this paper to study the tethered polymer problem are given in Section III. In Section IV we present our results, and finally, in Section V we give some concluding remarks.

II. DISCUSSION OF METHODS FOR HYDRODYNAMICS OF POLYMER SOLUTIONS

In this Section we give a brief overview of various methodologies for modeling hydrodynamics of soft matter systems, notably, polymer solutions (see also review by Duenweg and Ladd[24]). The various methods for computational hydrodynamics of polymer solutions can be divided in two major categories. The first are purely continuum methods that use

constitutive equations for the polymer solution. These models only apply at macroscopic scales, when the number of polymer chains in an elementary fluid flow volume is large, so that statistical averages of the chain conformations can be used as parameters in constitutive models of the time-dependent stress as a function of the strain rate history. The construction of such constitutive models is *ad hoc* and rather difficult in situations where conformations of the chains couple to an unsteady flow, as, for example, in the problem of turbulent drag reduction. Additionally, such continuum methods do not apply to situations where the dynamics of individual chains are of interest, such as a DNA molecule flowing through a micro-channel or DNA translocation through a pore. The second major category of methods explicitly simulates the motion of each polymer chain using some form of molecular dynamics. The simplest chain model is a dumbbell. Multi-bead representations of the chains are capable of complex chain conformations but require models for the bead-bead interactions. Such details of the polymer model are important for both physical fidelity and computational efficiency. For example, preventing chain-chain crossing can require stiff interactions for excluded volume terms, which in turn can lead to small time steps. There are also two major types of algorithms for dealing with the solvent. One represents the solvent *implicitly*, and the others use an *explicit* solvent. An implicit solvent is most efficient computationally, however, it can only be used if the fluid flow in the absence of the polymer is known analytically or can easily be pre-computed numerically (e.g., stationary flow), and if the polymer chains themselves do not alter the background flow.

A. Implicit Solvent: Brownian Dynamics

The most widely used implicit-solvent algorithm is Brownian dynamics[22], described in more detail in Section III A. The method involves solving first-order differential equations of motion for the positions of the beads with additional forces due to the presence of the solvent. These *solvent forces* can be separated into a *deterministic* portion, for which a (linear) analytical approximation is used, and a *stochastic* portion, which is assumed to be white noise. The fluctuation-dissipation theorem is used to set the magnitude of the stochastic forcing. Brownian dynamics relies on several assumptions usually valid in microfluidic applications. The first assumption is that of small Reynolds number laminar (usually stationary) flow adequately described by a linearized Navier-Stokes equation. The second assumption is

that hydrodynamic fields develop infinitely quickly relative to the rate at which the polymer conformation changes, so that a quasi-stationary approximation can be used to describe the perturbation of the flow field induced by the motion of the beads. This approximation leads to Stokes friction on single beads, as well as hydrodynamic interaction pairwise terms approximated with a long-range Oseen tensor as derived through an asymptotic ($t \to \infty$) analysis for point particles. The *free-draining* approximation of Brownian dynamics neglects these pairwise hydrodynamic interactions. The inclusion of pairwise hydrodynamic interactions leads to a matrix formulation of the fluctuation-dissipation theorem and therefore factorization of a matrix of the size of the number of beads is required at every time-step. Various numerical tools have been devised to avoid dense factorization[22,25–27], thereby reducing the cost of a single time step in Brownian dynamics with hydrodynamic interactions.

Brownian Dynamics should be distinguished from Langevin dynamics, in which second-order (Newton's) equations of motion are used for the beads, that is, both the bead velocities and positions are included as explicit degrees of freedom (but the solvent is still implicit)[28]. This assumes that there is a large separation of time-scales between the fluid degrees of freedom and the velocities of the beads, which is in fact only true if the beads are much denser than the solvent. Furthermore, a much smaller timestep necessary to resolve the faster dynamics (relaxation) of the bead velocities. Therefore, Langevin dynamics finds its use only when the solvent is represented explicitly, so that calculating the friction and stochastic forces no longer requires factorization of the mobility tensor.

An important advantage of Brownian dynamics is that it simulates the limit of zero Reynolds number exactly. It can also often exactly account for simple boundary conditions (e.g., flow in an infinite half plane) without resorting to approximations that truncate the flow field to a finite domain, such as the commonly-used periodic boundary conditions. Brownian dynamics is relatively easy to implement, however, complex boundary conditions, such as indentations or bumps on walls, requires care so that analytical approximations to the Oseen tensor that preserve the positive-definiteness of the diffusion tensor[29]. While the computational cost can rise rapidly as the number of beads is increased when direct implementations are used, novel schemes can be used to truncate the long-range hydrodynamic interactions and yield a linear dependence on system size, similarly to the handling of electrostatic interactions in spectral[26] and multipole methods[27].

B. Explicit Solvent: Continuum Methods

In order to capture the bi-directional coupling between the motion of the polymer and the flow around it, it is necessary to explicitly represent the solvent. The first level of approximation is to use a continuum description of the solvent assuming the applicability of the Navier-Stokes (NS) PDEs at small length scales. Typically an incompressible assumption is made, which is appropriate at sufficiently low Mach numbers if acoustic waves are not of interest. Additional approximations such as linearization or an iso-thermal approximation may be appropriate. The time-dependent (unsteady) NS equations can be solved by any of the numerous existing CFD algorithms, including explicit, implicit, or semi-implicit algorithms of varying level of complexity[30–32]. One of the advantages of the PDE formulation over particle methods is the ability to use powerful *adaptive mesh resolution* techniques that allow coarsening of the mesh away from the region of interest, here polymer chains. However, the case of complex boundary conditions such as needed, for example, in the handling of moving beads or flow through porous media, presents difficulties. An alternative to solving the Navier-Stokes PDEs is to use the Lattice-Boltzmann (LB) method[33], as discussed in Section III B. It requires small time steps limited by CFL-type conditions, however, each of the time steps is efficient. Recently, so-called entropic LB schemes have been developed that posses a discrete H-function, resulting in unconditional numerical stability even at high Reynolds numbers[34]. LB has been found competitive with NS solvers in many situations and has the further advantage that it is based on kinetic theory and allows a more detailed level of description than NS. An important advantage of LB solvers is also their ability to handle complex boundary conditions. Recently, Chen *et al.* have provided a detailed comparison between BD and LB simulations on a DNA model that shows that the LB method provides a reasonable description of the results of more precise BD simulations at low Reynolds numbers[35].

1. *Thermal Fluctuations*

Most continuum fluid dynamics methods are deterministic and thus do not include internal fluctuations of the hydrodynamic fields. Fluctuations become more important the smaller the length scale of interest, and are crucial for polymer flows. Including thermal

fluctuations in a continuum formulation has been carried out for both CFD and LB algorithms. The Landau-Lifshitz Navier Stokes (LLNS) equations include thermal fluctuations in the stress tensor but numerical schemes to solve them are not nearly as advanced as are the standard CFD solvers[30,36,37]. Fluctuations have been included in LB and do not pose any particular numerical problems[38]. Fluctuations have also been included in incompressible solvers in conjunction with the Immersed Boundary Method[32,39]. The ability to turn fluctuations on or off is an important advantage of continuum-based methods over particle methods.

2. Coupling with the Polymer Chains

Regardless of what continuum method is employed, it is necessary to couple that method to the MD description of the polymer chains. The simplest and most commonly used coupling scheme is to approximate the beads as points and assume for the solvent-induced force on the polymer beads the Stokes-Langevin form $\mathbf{F} = -6\pi R_H \eta \mathbf{v}_f + \mathbf{F}_S$, where $\mathbf{v}_f$ is an estimate of the local fluid velocity and $\mathbf{F}_S$ is an uncorrelated stochastic force whose magnitude obeys the fluctuation-dissipation theorem[31,40]. This approximation is similar to that in Brownian dynamics, namely, Stokes law is only valid in quasi-static continuum situations, relying on the separations of time and length scales which are usually only marginally separated in realistic situations. Typically the strength of the coupling, R_H, is empirically tuned to reproduce experimental measurements. The coupling can also be dealt with when the beads occupy an actual volume, free of fluid. Then stick or slip boundary condition at the surface of the beads are employed, as in both NS[30] and LB[33] simulations of colloidal dispersions. However, these methods are rarely used in polymer simulations due to the complexity when many moving particles are involved, because, the grid size needs to be smaller than the bead size and may need to be adaptively changed when the bead moves.

A different alternative is provided by the Immersed Boundary method[32], where the fluid occupies the whole space and the particles, represented as immersed structures, move together with the fluid with a velocity that is a localized average of the fluid velocity. This eliminates the bead inertia from the problem and the need to explicitly enforce boundary conditions on the surface of the beads. The method can be seen as an alternative to Brownian dynamics that correctly captures *time-dependent* momentum transport in the fluid by ex-

plicitly representing the fluid flow, and also includes thermodynamically-consistent thermal fluctuations[39].

C. Explicit Solvent: Particle Methods

An alternative to continuum methods is to use a particle representation of the fluid. The most detailed description is a MD simulation of both the fluid and the solvent. Unlike the classical NS equations, MD automatically and correctly includes fluctuations, internal fluid structure, diffusion, and non-linear transport. Particle methods are also typically simple to implement and can easily accommodate complex boundary conditions.Typically a truncated repulsive Lenard-Jones potential is used for the solvent-solvent interactions. However, even with massive parallelization such MD simulations are limited to short total times and therefore efforts have been made to coarse-grain the solvent to a mesoscopic representation. There, the fluid particles are no longer representative of solvent molecules, but are larger having different dynamics and interactions with each other. However, the viscosity and the stress fluctuations in the solvent must be reproduced correctly. There are mesoscopic particle solvents of progressively decreasing level of microscopic fidelity, and thus increasing efficiency. The handling of the coupling between the solvent and the beads is a separate issue, like for continuum solvents. A particle solvent may be coupled to a polymer chain by including explicit short-ranged solvent-bead continuous[41] or hard-spheres[17] interaction potentials. Efficiency can further be gained by coarse graining the bead-solvent interactions as well, typically using the same ideas as used to coarse grain the solvent-solvent interactions[42,43]. Dissipative Particle Dynamics (DPD)[44] further coarsens the solvent molecules to obtain a system of weakly-repulsive spheres interacting with a mixture of conservative, stochastic, and dissipative forces. The conservative forces can be used to reproduce the solvent equation of state, while the dissipative forces model viscous friction. The stochastic forces act as a thermostat that ensures detailed balance and correct thermal fluctuations in the DPD fluid. The method has great flexibility and requires significantly less solvent particles and larger time-steps than classical MD, however, it still requires costly integration of differential equations of motion for each of the solvent particles. Such integration of ODEs can be avoided by using a kinetic Monte Carlo method, such as Direct Simulation Monte Carlo (DSMC), to represent the solvent-solvent interactions. The idea is to use stochastic conser-

vative collisions between nearby solvent particles to represent the exchange of momentum and energy. Both multi-particle collisions[42,43] and binary collisions[17] have been used, as described in Section III C. The computational efficiency comes at the cost of neglecting the structure of the solvent, as in continuum methods. Recently a new Stochastic Hard-Sphere Dynamics method has been proposed that also uses uncorrelated stochastic binary collisions but still produces a non-trivial fluid structure and a thermodynamically-consistent non-ideal equation of state, similar to those of a DPD fluid[45].

D. Coupled Methods

Methods that combine several of the techniques described above into a single *concurrently coupled* simulation can take advantage of their region of validity. Such a simulation may involve several *levels* each with a different level of microscopic detail. For example, molecular dynamics with complete atomistic detail and realistic potentials may be used for the polymer chain(s) and nearby solvent. The solvent can then be coarse grained to a mesoscopic particle fluid sufficiently far from any chains. The particle method can then be coupled to an explicit fluctuating hydrodynamic description with a fine grid, for example, LB or a fluctuating NS solver. Finally, the hydro grid can be adaptively coarsened in regions even farther from the chain, and a non-fluctuating continuum solver used. This last macroscopic level can use a different method from the fluctuating hydrodynamics level, for example, it could be an incompressible NS solver. Much remains to be done to enable a truly multiscale simulation capable of bridging from microscopic to macroscopic length and time-scales[46,47].

III. SIMULATION METHODS

In this Section we describe in further technical detail the three different techniques we apply to the tethered polymer problem. The majority of the methodology has been previously published so here we only summarize the essential points and cite the relevant works.

A. Brownian Dynamics

Details of the DNA model and Brownian dynamics simulation method that we use can be found in Refs.[22,25]. We discretize a double-stranded DNA molecule into a bead-spring chain composed of N_b beads of radius $R_b = 77$nm (the unit of length, 1 $l.u.$ = 77nm) connected by $N_s = N_b - 1$ entropic springs. Each spring represents a DNA segment of 4850 base pairs, so that $N_b = 11$ corresponds to a stained λ-DNA, which has a contour length of 21 μm. In Brownian dynamics, a force balance on this chain leads to a stochastic differential equation for the dynamics of the chain[48],

$$\Delta\mathbf{R} = [\mathbf{U} + \frac{\mathbf{D}\cdot\mathbf{F}}{k_BT} + \frac{\partial}{\partial\mathbf{R}}\cdot\mathbf{D}]\Delta t + \sqrt{2}\mathbf{B}\cdot\Delta\mathbf{W} \tag{1}$$

where $\mathbf{R}$ is the vector containing bead positions, $\mathbf{R} = \{\mathbf{r}_1, ..., \mathbf{r}_N\}$, $\mathbf{U}$ is the unperturbed velocity field at the bead centers, k_B is Boltzmann constant, T is absolute temperature, $\mathbf{F}$ is the non-hydrodynamic and non-Brownian forces, and $\mathbf{D} = \mathbf{B}\cdot\mathbf{B}^T$ is the diffusion tensor. The components of $\Delta\mathbf{W}$ are obtained from a real-valued Gaussian distribution with mean zero and variance dt. In a unbounded space, the hydrodynamic interactions (HI) enter the chain dynamics through the diffusion tensor,

$$\mathbf{D}_{ij} = k_BT[(6\pi\eta a)^{-1}\mathbf{I}\delta_{ij} + \mathbf{\Omega}_{ij}] \tag{2}$$

where η is the viscosity of the solvent, a is the bead hydrodynamic radius, $\mathbf{I}$ is the unit tensor, δ_{ij} is the Kronecker delta, and $\mathbf{\Omega}$ is the HI (Stokeslet or Oseen) tensor.

Recent work has provided evidence of hydrodynamic coupling to the wall and experimental validation of the use of point-particle (Stokeslet) hydrodynamic interactions (HI) to describe the motion of Brownian particles near a surface[49]. Therefore, it is essential to have wall corrected HI in the simulation to capture the dynamics of a tethered chain correctly. In a bounded space, like near a solid wall, the HI tensor is modified to,

$$\mathbf{\Omega}_{ij} = (1 - \delta_{ij})\mathbf{\Omega}^{OB}(\mathbf{r}_i - \mathbf{r}_j) + \mathbf{\Omega}^{W}(\mathbf{r}_i - \mathbf{r}_j) \tag{3}$$

where $\mathbf{\Omega}^{OB}$ is the free-space diffusion tensor, and $\mathbf{\Omega}^{W}$ is the correction which accounts for the no-slip constraint on the wall. The solution for a Stokeslet above a flat plate given by Blake allows us to calculate $\mathbf{\Omega}^{W}$ exactly[50]. In a square channel or complex geometries, we need to solve this problem numerically with a finite element method to determine $\mathbf{\Omega}^{W}$ at

a grid of points[8]. Based on this description of near-wall HI, Jendrejack *et al.*[51] predicted that the DNA molecules migrate away from the wall in shear flow, leading to the formation of depletion layers in the near wall region. This prediction has been verified in recent experiments of dilute DNA solutions undergoing pressure-driven flow in microchannels[52,53]. In different works, Delgado-Buscalioni used a hybrid particle-continuum model method to describe HI[15] and Schroeder *et al.* used unbounded space HI[14] to study the motion of a tethered chain.

We further assume that the chain is ideal (no self-excluded volume interactions between different beads). The entropic springs connecting the beads obey a worm-like chain law

$$\mathbf{F}_{ij}^{s} = \frac{k_B T}{2b_k}[(1 - \frac{|\mathbf{r}_j - \mathbf{r}_i|}{N_{k,s} b_k})^{-2} - 1 + \frac{4|\mathbf{r}_j - \mathbf{r}_i|}{N_{k,s} b_k}]\frac{\mathbf{r}_j - \mathbf{r}_i}{|\mathbf{r}_j - \mathbf{r}_i|}, \tag{4}$$

where b_k is the Kuhn length for DNA and $N_{k,s}$ is the number of Kuhn lengths per spring. The physical confinement is taken into account through an empirical bead-wall repulsive potential of the form

$$U_i^{wall} = A_{wall} b_k^{-1} \delta_{wall}^{-2} (h_i - \delta_{wall})^3, \tag{5}$$

when $h_i < \delta_{wall}$, where h_i represents the perpendicular distance of bead i from the wall, δ_{wall} is the cut-off distance. In this work, we choose $A_{wall} = 25 k_B T$ and $\delta_{wall} = b_k N_{k,s}^{1/2}/2 = 0.24$ μm. All of the parameters $\{a, b_k, \nu\}$ are the same as used in previous work, where it has been shown to successfully reproduce the static and dynamic properties of DNA with contour length $10\mu m - 126\mu m$[8,25]. For each parameter set, the sample size is 30 chains unless otherwise specified. All results are presented for DNA at room temperature in a solvent with a viscosity of 1 cP .

To study the dynamics of a tethered chain, beads are labeled from 1 to $N_b + 1$, starting from the tethered point, as illustrated in Fig. 1. The fluid velocity in the flow direction z is a linear function of distance from the wall in the gradient direction x, $v_z = \dot{\gamma} x$, where $\dot{\gamma}$ is the shear rate, and $v_x = 0$ and $v_y = 0$. Following common experimental practice, the longest relaxation time is calculated by allowing a chain that is initially stretched using a large shear rate to relax to equilibrium. Near equilibrium, the relaxation time is determined by an exponential decay fit the chain extension along the stretch direction,

$$\langle \bar{X}^2 \rangle = (\bar{X}^2(0) - \langle \bar{X}^2 \rangle_{eq}) \exp(-\frac{t}{\tau}) + \langle \bar{X}^2 \rangle_{eq}. \tag{6}$$

An exponential fit to the autocorrelation of the chain extension (relative to equilibrium) parallel to the wall gives similar results. The relaxation time for our λ-DNA is estimated to

be 0.59s at room temperature, which is in good agreement with the experimental result of 0.51s[12] after extrapolating the viscosity to 1 cP.

B. Lattice-Boltzmann

In addition to Brownian Dynamics, we examine the short time correlations of a tethered polymer in a uniform shear flow using a hybrid Lattice Boltzmann (LB) and Molecular Dynamics (MD) code based on the method by Ahlrichs and Dunweg[23]. The Lattice Boltzmann method is a mesoscopic approach to fluid flow calculation and is based on a discrete version of the Boltzmann equation with enough detail to recover hydrodynamic behavior. The LB equation describes the evolution of a single-particle distribution function, $f_i(\mathbf{x}, t)$, which is the mass density of particles moving with velocity $\mathbf{e}_i$ at a time t and position $\mathbf{x}$ on a cubic lattice,

$$f_i(\mathbf{x} + \mathbf{e}_i \Delta t, t + \Delta t) = f_i(\mathbf{x}, t) + \sum_j A_{ij} \left[f_j(\mathbf{x}, t) - f_j^{eq}(\mathbf{x}, t) \right]. \tag{7}$$

The set of velocities $\mathbf{e}_i$ is discrete and chosen such that $\mathbf{x} + \mathbf{e}_i \Delta t$ always remains a lattice site. The last term describes the collision process in which the distribution function relaxes to a local equilibrium, for which we utilize the BGK (Bhatnagar-Gross-Krook) approximation to the collision operator, $A_{ij} = -\tau^{-1}\delta_{ij}$, where τ is a relaxation time. The macroscopic hydrodynamic quantities, density ρ, momentum $\mathbf{j} = \rho\mathbf{u}$, and momentum flux $\mathbf{\Pi}$, are computed from moments of the particle distribution function,

$$\rho = \sum_i f_i, \ \mathbf{j} = \sum_i f_i \mathbf{e}_i, \text{ and } \mathbf{\Pi} = \sum_i f_i \mathbf{e}_i \otimes \mathbf{e}_i. \tag{8}$$

The equilibrium distribution depends on the macroscopic variables and its form is given by

$$f_i^{eq}(\mathbf{x}, t) = w_i \rho \left[1 + \frac{\mathbf{e}_i \cdot \mathbf{u}}{c_s^2} + \frac{(\mathbf{e}_i \cdot \mathbf{u})^2}{2c_s^4} - \frac{\mathbf{u}^2}{2c_s^2} \right], \tag{9}$$

where the weights w_i depend on the particle velocity discretization and are determined by mass and momentum conservation. The lattice sound speed is $c_s = \Delta x/\sqrt{3}\Delta t$, where Δx is the lattice spacing. In this work we solved the distribution function on the standard D3Q19 lattice[54] where the 19 particle velocity components consist of one rest particle, the 6 nearest neighbors in a simple cubic lattice, and the 12 next nearest neighbors in the [110] directions. The corresponding weights are 1/3, 1/18, and 1/36. The LB method avoids the additional

mathematical complexities of Navier-Stokes PDE solvers and is straightforward to parallelize efficiently. Using a Chapman-Enskog expansion, the lattice-Boltzmann equation can recover the Navier-Stokes equations for small Mach and Knudsen numbers, and, within these limits it is second-order accurate in space and time. Compared to the other two methods we apply to the tethered polymer problem, BD and SEDMD, LB is less efficient in this case since it solves for the solvent in the entire domain, even relatively far from the polymer chain.

In the LB calculations, the polymer is represented by 25 point particles joined by finitely extendable nonlinear elastic (FENE) springs and interact through a repulsive Lennard-Jones potential among each other and with the walls. Solvent fluctuations are incorporated by adding a stochastic term to the right hand side of the LB equation. This term introduces fluctuations into the momentum flux in a manner that satisfies the fluctuation-dissipation theorem[54]. Coupling between the LB for the solvent and the MD for the solute is achieved through Stokes drag forces and white-noise stochastic forces acting on the monomers. The first monomer in the chain is tethered to the stationary lower wall in a domain having 36, 22, and 24 lattice sites in the streamwise, spanwise, and wall normal directions. The streamwise and spanwise directions are periodic and the bounding upper wall moves with constant velocity, providing the uniform shear.

C. Stochastic Event-Driven Molecular Dynamics

In addition to Brownian dynamics and Lattice-Boltzmann, we have also applied a purely particle-based method to the tethered polymer problem. The Stochastic Event-Driven Molecular Dynamics (SEDMD) algorithm introduced in Ref. [17] combines Event-Driven Molecular Dynamics (EDMD) for the polymer particles with Direct Simulation Monte Carlo (DSMC)[55] for the solvent particles. In SEDMD, the polymers are represented as chains of hard spheres tethered by square wells. The solvent particles are realistically smaller than the beads and are considered as hard spheres that interact with the polymer beads with the usual hard-core repulsion. The algorithm processes true (deterministic, exact) binary collisions between the solvent particles and the beads, without any approximate coupling or stochastic forcing. However, the solvent particles themselves do not directly interact with each other, that is, they can freely pass through each other as for an ideal gas. Deterministic collisions between the solvent particles are replaced with momentum- and energy-conserving

stochastic collisions between nearby solvent particles. This gives realistic hydrodynamic behavior and fluctuations in the solvent, with tunable viscosity and thermal conductivity, but without internal fluid structure. A recent modification of the DSMC algorithm can be used to achieve a non-ideal equation of state for the stochastic solvent that is thermodynamically-consistent with the density fluctuations[45].

Hard-sphere models of polymer chains have been used in EDMD simulations for some time[56–58]. These models typically involve, in addition to the usual hard-core exclusion, additional *square well* interactions to model chain connectivity. Recent studies have used square well attraction to model the effect of solvent quality[59]. Even more complex square well models have been developed for polymers with chemical structure and it has been demonstrated that such models, despite their apparent simplicity, can successfully reproduce the complex packing structures found in polymer aggregation[57,58]. Here we use the simplest model of a polymer chain, namely, a linear chain of N_b particles tethered by unbreakable bonds. This is similar to the commonly-used freely jointed bead-spring FENE model model used in time-driven MD. The length of the tethers has been chosen to be $1.1D_b$, where D_b is the diameter of the beads.

Several particle methods for hydrodynamics have been described in the literature, such as MD[60], dissipative particle dynamics (DPD)[44], and multi-particle collision dynamics (MPCD)[41,61]. Molecular dynamics is the most accurate model of the fluid structure and dynamics, however, it is very computationally demanding due to the need to integrate equations of motion with small time steps Δt and calculate interparticle forces at every time step. The key idea behind DSMC is to replace deterministic interactions between the particles with stochastic momentum exchange (collisions) between nearby particles. The standard DSMC[55] algorithm starts with a time step where particles are propagated advectively, $\mathbf{r}_i^{'} = \mathbf{r}_i + \mathbf{v}_i \Delta t$, and sorted into a grid of cells. Then, a certain number $N_{coll} \sim \Gamma_c N_c (N_c - 1)\Delta t$ of *stochastic conservative collisions* are executed between pairs of particles randomly chosen from the N_c particles inside the cell. For mean free paths comparable to the cell size, the grid of cells should be shifted randomly before each collision step to ensure Galilean invariance. The collision rate Γ_c and the pairwise probability distributions are chosen based on kinetic theory.

In SEDMD the polymer chains and the bead-solvent interactions are handled using hard-sphere event-driven molecular dynamics (EDMD)[56,59,62,63] instead of the time-driven MD

(TDMD) widely used for continuous potentials. The essential difference between EDMD and TDMD is that EDMD is asynchronous and there is no time step, instead, collisions between hard particles are explicitly predicted and processed at their exact (to numerical precision) time of occurrence. Since particles move along simple trajectories (straight lines) between collisions, the algorithm does not waste any time simulating motion in between events (collisions). SEDMD combines time-driven DSMC with EDMD by splitting the particles between ED particles and TD particles. Roughly speaking, only the polymer beads and the DSMC particles surrounding them are treated asynchronously as in EDMD. The rest of the DSMC particles that are not even inserted into the event queue. Instead, they are handled using a time-driven (TD) algorithm very similar to that used in traditional DSMC.

In three dimensions, a very large number of solvent particles is required to fill the simulation domain. The majority of these particles are far from the polymer chain and they are unlikely to significantly impact or be impacted by the motion of the polymer chain. We therefore approximate the behavior of the solvent particles sufficiently far away from any polymer beads with that of a quasi-equilibrium ensemble. In this ensemble the positions of the particles are as in equilibrium and the velocities follow a local Maxwellian distribution whose mean is the macroscopic local velocity. These particles are not simulated explicitly, rather, we can think of the polymer chain and the surrounding DSMC fluid as being embedded into an infinite reservoir of DSMC particles which enter and leave the simulation domain following the appropriate distributions. Using such open or *stochastic boundary conditions* dramatically improves the speed, at the cost of small errors due to truncation of hydrodynamic fields. This truncation can be avoided by coupling DSMC to a continuum fluctuating hydrodynamic solver[46].

We have made several runs for different polymer lengths and also bead sizes. One set of runs used either $N_b = 25$ or 50 large beads each about 10 times larger than a solvent particle. Another set of runs used either $N_b = 30$ or 60 small beads each identical to a solvent particle, with faster execution but nearly identical results. In the simulations reported here we have used rough wall BCs for collisions between DSMC and non-DSMC particles[17]. This emulates a non-stick boundary condition at the surface of the polymer beads. Using specular (slip) conditions lowers the friction coefficient, but does not qualitatively affect the behavior of tethered polymers. All of the runs used open boundary conditions, where about 15^3 DSMC cells around each bead were explicitly simulated. Note that for (partially) collapsed

polymer chains the total number of explicitly simulated cells is much smaller than $15^3 N_b$. The $N_b = 30$ runs were run for about $6000\tau_0$ relaxation times, and such a run takes about 6 days on a single 2.4GHz Dual-Core AMD Opteron processor. Even for such long runs the statistical errors due to the strong fluctuations in the polymer conformations are large, especially for correlation functions at long time lags $t > \tau$.

IV. RESULTS

The main goal of our paper is to reinvestigate the tethered chain problem through extensive long time simulations (thousands of longest relaxation time of the tethered polymer, τ) involving different representations of polymer and solvent, including Brownian dynamics[22] (BD), the Lattice Boltzmann method[23] (LBM), and a recent Stochastic Event-Driven Molecular Dynamics[17] (SEDMD) algorithm. In this section we present comparison results from our simulations. More extensive results for the tethered polymer problem obtained using the SEDMD algorithm are presented in Ref. [17]. Since the three different methods that we use give similar results and Brownian Dynamics is the fastest methodology, the majority of the results we present will be from BD simulations with $N_b = 11$ ($N_s = 10$), unless otherwise indicated. Of the three methods used here, LB is the slowest and thus the LB results are of more limited duration. We emphasize that direct computational comparison between the methods is unfair. Most significantly, the LB runs use periodic boundary conditions and have to fill the whole simulation domain with explicit solvent (lattice points). By contrast, the SEDMD runs use open boundaries and thus use much less explicit solvent, whereas the Brownian dynamics does not use an explicit solvent at all.

Doyle *et al.* proposed a cyclic dynamics mechanism for a tethered polymer chain in shear flow (Fig. 1) based on Brownian dynamics simulation results[12]. According to this scenario, when thermal fluctuations cause motion in the gradient direction x (from state 1 to state 2), the chain is driven away from the wall and experiences higher hydrodynamic drag. This leads to further stretching and an increase of the extension in the flow direction z (state 3). Due to the finite extensibility of the chain, the extension in the z direction is finite and depends on the shear rate and chain properties. After stretching, the coupled torque of the hydrodynamic drag and spring forces will rotate the chain towards the wall (state 4). As the chain get closer to the wall, the flow velocity decreases and entropic recoiling becomes

dominant, resulting in a decrease of the z extension (state 1). The tethered chain could take other dynamical paths than following the one described above, such as restretching or recoiling after state 2 by random motion in $-x$ and $-z$ direction, respectively.

In Fig. 2 we show the probability distribution function (pdf) $\rho(z, x)$ of the end bead in the $z-x$ plane at $Wi = 0$ and $Wi = 2$ for the three different methods. The results are presented in dimensionless units by normalizing the unit of length by the average radius of gyration in the x direction at $Wi = 0$. Here, again, we want to emphasize that we are not expecting perfect match between methods. In particular, the different methods implement different effective boundary conditions at the wall surface. In Brownian dynamics, an essentially reflective boundary condition appears, while in the case of a hard-sphere chain a perfectly reflective boundary condition is appropriate. For the LB runs an intermediate case appears, where the repulsion from the wall is stronger than hard spheres but still finite-ranged. These boundary effects are clearly visible in the results in Fig. 2, where the BD results show a depletion layer near the wall where as the SEDMD and LB results show the bead spending more time near the wall.

In Fig. 3 we compare the dependence of the relaxation times $\tau_{x/y/z}$ along the three different axes on the flow rate among the three different methods. The figure shows reasonable agreement between the different techniques, especially considering the large errors inherent in determining relaxation times. We calculate the relaxation times by fitting an exponential decay to the intermediate portion of the autocorrelation function $0.2 < C(t) < 0.8$ of the position of the end bead along the three coordinate axes. The LB calculations use periodic boundaries with a narrower box in the spanwise (y) direction than in the streamwise (x) direction, which makes the relaxation times $\tau_x(Wi = 0)$ and $\tau_y(Wi = 0)$ unequal, as they must be by symmetry. We have scaled $\tau_y(Wi)$ (the shorter axes) in the LB results by a constant factor so as to correct this strong boundary effect at $Wi = 0$. Among the three relaxation times, the relaxation in the direction perpendicular to the wall τ_z is the shortest, even for no flow. Note than in this work, following Ref. [17], the relaxation time along the flow direction τ_x is used to define the internal relaxation time and thus Wi when comparing among the different methods. Note also that it is τ_x that seems to get most strongly reduced as Wi increases.

To study the time scale associated with the fluctuating process (cycle) quantitatively and to find the correlation between different chain segments, we calculated the cross-correlation

functions (CCF) of beads' positions. We also calculated the power spectral density (PSD) in search of periodicity. The CCF and PSD are the natural tools for examining the relationship between two time dependent random variables in the time and frequency domain respectively. The mean-removed CCF of two time series $\alpha(t)$ and $\beta(t)$ is defined as

$$C_{\alpha\beta}(T) = \frac{E[(\alpha(t+T) - \bar{\alpha})(\beta(t) - \bar{\beta})]}{\sigma_\alpha \sigma_\beta} \tag{10}$$

where $\bar{\alpha} = E(\alpha)$ is the mean, $\sigma_\alpha^2 = E(\alpha^2) - [E(\alpha)]^2$ is the standard deviation, and T is the time lag. A significant peak in the CCF at lag T indicates that $\alpha(t)$ is correlated to $\beta(t)$ when delayed by time T. In the frequency domain, the PSD is the norm of the Fourier transform of the CCF,

$$S_{\alpha\beta}(\nu) = \left\| \int_{-\infty}^{\infty} C_{\alpha\beta}(T) exp(-2i\pi\nu T) dT \right\| \tag{11}$$

Note that this is the standard definition used in the engineering literature, and here the frequency $\nu = 1/T$ is actual frequency (inverse period) rather than angular frequency $\omega = 2\pi\nu$. To produce a PSD with accurate sampling around interesting frequencies, long simulation times and a high sampling frequency are essential. We examined various choices of variables to represent the motion of the chain and have found little qualitative difference between them. We have chosen the position of the end bead $r_{N_b} = (x, y, z)$ as be the best option[17]. Extensive computational efforts have been undertaken to determine the CCF and PSD of the end bead coordinates as function of chain length N and shear flow parameter Wi.

The CCF $C_{zx}(t)$ of the end bead at various Wi is shown in Fig. 4(a). The shape of the CCF is consistent with the cyclic dynamics mechanism proposed by Doyle. Clearly, in the absence of flow, $Wi = 0$, the movements in the x and z directions are uncorrelated on all time scales. When shear flow is introduced, the movements in flow direction and gradient direction are coupled together due to the nature of the flow and the finite extensibility of the chain, as reflected in the rise of a prominent peak in the CCF. When thermal motion in $+x$ direction occurs, the chain will be stretched with an increase in $+z$, which leads to a positive correlation. Similarly, when motion in $-x$ direction is introduced, the chain will recoil in the $-z$ direction as the drag decreases, which also leads to a positive correlation. As expected, the larger the shear rate, the greater the correlation. There's only one significant peak in the long time correlation function, shown in the inlet of Fig. 4(a), which suggests that all correlations are short-lived and not periodic.

Turning attention to the correlation between different chain segments, Fig. 5 shows the CCFs of several beads along the chain at $Wi = 2$. One striking feature is that for beads sufficiently far from the tether all curves pass the time axis at the same time lag. The fact that all CCFs have the same shape indicates that a common movement pattern exists for the whole chain. The inset in Fig. 5(a) shows the CCFs of the x coordinates of different beads. Although the correlation decays as the distance along the chain increases, it confirms that all beads move in a cooperative manner, indicated by the fact that the peak positions are all at zero time lag. The CCF for the end bead for various chain lengths are compared in Fig. 5(b), to show that there is no fundamental difference between different chain lengths, ranging from 20 μm ($N_s = 10$) to 80 μm ($N_s = 40$). We have also established that these results are insensitive to the cut-off distance and the magnitude of the repulsive potential between the wall and chain segments.

In Fig. 6 we compare the cross-correlation function $C_{zx}(t)$ at $Wi = 2$ among the three different methods: Brownian Dynamics, Lattice-Boltzmann, and Stochastic Event-Driven Molecular Dynamics. In particular, our goal is to verify the pervasive assumption that the dynamics of polymer chains in shear flow is essentially universally *quantitatively* determined by Wi for a wide range of flexible chains. Furthermore, it is important to cross-validate the different methods against each other, given that each of them makes certain assumptions and has somewhat different range of applicability. The results in Fig. 6 indeed show reasonable agreement between the different methods. Perfect agreement is not expected because the polymer models are different among the different methods.

The cross-correlations we measure are not consistent with periodic motion. The PSD calculation does not show discernible peaks either, as shown in Fig. 4(b). All that we can reliably extract from the results is that the response of the chain to a large thermal fluctuation (the "cycle") is reproducible for *short* times, and we find no evidence of sustained correlations (oscillations) at times longer than the internal relaxation time of the chain. For a free chain in shear flow, where rotations of the chain are possible, one can count the number of tumbling events per unit time and define that as a cycling time. The distribution of the delays between successive tumbling events is itself important. If this distribution is sharply peaked, that would be consistent with a periodic motion with a well-defined period. If the distribution is exponential, this would indicate a Poisson-like tumbling process. Several recent works have proposed an exponential distribution for the delay between successive tumblings[7,19,20].

Furthermore, the tumbling time was found to be related to the internal relaxation time of the chain[19,20]. For tethered chains, we cannot even identify and count a unique event such as tumbling and thus we cannot extract a repetition frequency for the "cycle".

In Appendix A, we analytically calculate the CCF for a Brownian particle tethered to the origin with a harmonic spring and subjected to shear flow. This simple dimer model qualitatively reproduces the features we see in the CCF for the tethered chains, namely, a single peak at $t \sim \tau$ of width $\sim \tau$ and height $\sim Wi$. Better quantitative agreement is obtained when a nonlinear spring and a hard wall surface are also included (without hydrodynamics). The PSD for the dimer model shows no peaks and there is only a single time-scale in the dynamics, namely, the intrinsic relaxation time τ. Furthermore, the analytical form of the CCF shows that by a slight modification of a tunable parameter one can obtain a CCF fully-consistent with our numerical results for longer chains. This analytical CCF has an analytical PSD that does show a broad peak at small frequencies $\nu\tau \sim 0.1$, very similar to the previously reported peaks used to justify the claims to periodicity in the chain motion[14,15,18]. This peak is weak and broad even when plotted on a logarithmic axes and its exact shape and maximum will vary depending on the particular model, variables used in calculating the PSD, Wi, the definition used for calculating τ and Wi, etc. We therefore believe that its interpretation as evidence of periodic motion is not justified.

The calculations in Appendix A for a dimer in shear flow also demonstrate that a qualitatively similar behavior is observed even without hydrodynamic interactions. Our results from Brownian Dynamics simulations in the free-draining limit confirm this and show that the HI do not affect the results significantly, so long as the relaxation time is recalculated when computing Wi. In the tethered case, we believe that the competition between frictional and elastic restoring forcing dominates and the hydrodynamic interactions are a weak perturbation. Therefore, it is not surprising that the proper inclusion of hydrodynamic interactions is not essential for the tethered polymer problem, as reasoned theoretically for a free chain in shear flow in Ref. [20].

V. CONCLUSIONS

We studied the dynamics of a polymer molecule tethered to a hard wall and subjected to a shear flow. We found consistent results among three methods utilizing different represen-

tations of the solvent, Brownian Dynamics (BD), Lattice-Boltzmann (LB), and Stochastic Event-Driven Molecular Dynamics (SEDMD). Specifically, BD implicitly represents the solvent, LB explicitly represents the solvent flow on a discrete lattice, and SEDMD utilizes a particle-based solvent. The three methods also utilized different polymer chains, namely, the BD simulations used a worm-like chain, the LB simulations used a FENE-LJ chain, and for SEDMD we used a tethered chain of hard spheres.

The correlation functions of the position of the end bead question the existence of periodic motion, as previously suggested. The cross-correlation function between the bead positions along the flow and gradient directions shows a single peak indicative of a fluctuation-dissipation cycle of duration comparable to the relaxation time of the polymer. The corresponding Fourier representation, the power-spectral density, shows no peaks. We find that neither the chain length of the polymer N, nor the dimensionless shear rate Wi, qualitatively alter the results, and in the Appendix we give some calculations for a very simple model of a dimer in shear flow that reproduces the essential features of the observed peak in the cross-correlation function.

While our conclusions are rather different from other authors, our results are statistically consistent with those presented in the literature. Specifically, the shape and position of the peaks in the cross-correlation functions are very similar to reported results, however, we did not observe large oscillations in the CCFs previously identified as signatures of periodic motion[15]. We believe that this is due to the requirement of very long simulation times to obtain good statistics for the time-correlation functions at long time lags, as necessary to establish periodicity. Not all previous studies have been able to reach sufficiently long simulation times. Another important point we clarified is that maxima in the power-spectral density does not necessarily indicates a periodic motion, which we demonstrate in Appendix A using an analytic dimer model. Namely, an analytical shape is suggested by the dimer calculations that can exhibit peaks very similar to those reported in the literature through small adjustments of a tunable parameter, whose appropriate value likely depends on details of the model used and the exact variables used in the calculations of the power spectrum. Furthermore, different if not conflicting ways have been used to define and calculate the "cycling time", without properly distinguishing between the duration of a cycle and the interval between cycles. Even more importantly, the very concept of a cycle in the chain motion as a well-defined countable event, analogous to the case of a free chain in shear

flow, should be questioned. Our results are consistent with a simple traditional picture of continuous thermal fluctuations dissipated by deterministic friction, leading to exponentially-decaying correlation functions.

Acknowledgments

The work of A. Donev, T. Weisgraber and B. Alder was performed under the auspices of the U.S. Department of Energy by Lawrence Livermore National Laboratory under Contract DE-AC52-07NA27344. Y. Zhang, M. Graham, and J. de Pablo acknowledge the support from the University of Wisconsin-Madison Nanoscale Science and Engineering Center funded by the National Science Foundation (DMR-0425880).

Appendix A: DIMER IN SHEAR FLOW

In this Appendix we analytically and numerically consider the case of a Brownian particle attached to the origin with a harmonic spring with stiffness $k = \kappa\zeta$, where ζ is the friction coefficient, subject to shear flow, $v_x = \dot{\gamma}y$. If additionally we include a hard wall at $y = 0$ such that the random walk is restricted to the upper half-space, $y > 0$, we are essentially considering a tethered polymer chain composed of two beads. Note that this problem is essentially two-dimensional.

The overdamped Langevin equations for the particle coordinates are

$$\begin{aligned} \dot{x} &= \dot{\gamma}y - \kappa x + F_x \\ \dot{y} &= -\kappa y + F_y, \end{aligned}$$

where F denotes the random forcing. After performing a Fourier transform in time, we get the solution in Fourier space

$$\begin{aligned} \hat{x} &= \frac{(i\nu + \kappa)\hat{F}_x + \dot{\gamma}\hat{F}_y}{(i\nu + \kappa)^2} \\ \hat{y} &= \frac{\hat{F}_y}{(i\nu + \kappa)}, \end{aligned}$$

from which we can obtain all cross-correlation functions using the identities $\left\langle \hat{F}_x{}^\star \hat{F}_x \right\rangle = \left\langle \hat{F}_y{}^\star \hat{F}_y \right\rangle = \alpha$ and $\left\langle \hat{F}_x{}^\star \hat{F}_y \right\rangle = 0$. In particular, we obtain the monotonically-decreasing

non-normalized PSD

$$\tilde{S}_{xy}(\nu) = \left\|\hat{C}_{xy}\right\| = \|\langle \hat{x}^{\star}\hat{y}\rangle\| = \frac{\alpha\dot{\gamma}}{(\nu^2+\kappa^2)^{3/2}},$$

and, after an inverse Fourier transform, the non-normalized CCF

$$\tilde{C}_{xy}(t) = \begin{cases} \alpha\dot{\gamma}e^{-\kappa t}(2\kappa t+1)/(4\kappa^2) \text{ for } t \geq 0 \\ \alpha\dot{\gamma}e^{\kappa t}/(4\kappa^2) \text{ for } t < 0 \end{cases}.$$

In the case of no shear flow, $\dot{\gamma} = 0$, we obtain that $\tilde{C}_{xx}(t) = \alpha e^{-\kappa|t|}/(2\kappa)$, showing that the relaxation time is $\tau = \kappa^{-1}$ and thus $Wi = \dot{\gamma}/\kappa$. For the harmonic spring dimer the relaxation time does not depend on Wi. The cross-correlation function shows a single peak at $t_{max} = (2\kappa)^{-1} = \tau/2$, and after proper normalization, $C_{xy}(t) = \tilde{C}_{xy}(t)/\sqrt{\tilde{C}_{xx}(t=0)\tilde{C}_{yy}(t=0)}$, the height of the peak in the CCF is found to be

$$C_{xy}^{max} = C_{xy}(\tau/2) = \frac{\sqrt{2}e^{-1/2}\,Wi}{\sqrt{2+Wi^2}}. \tag{A1}$$

This analytically-solvable dimer model, even without a hard wall, reproduces the characteristics of the CCF that we observe for tethered polymer chains in shear flow. Specifically, $C_{xy}(t)$ has an asymmetric peak of width $\sim \tau$ centered at $t = \tau/2$ and height $\sim Wi$. There is no periodicity in the motion of the dimer and no "cycling" time-scale other than the intrinsic relaxation time τ.

The dimer problem can no longer be solved analytically if a hard wall is present or if the spring is non-linear (e.g., FENE or worm-like). We can, however, study the dimer with a non-linear spring and/or in the presence of a hard wall numerically using Brownian Dynamics (without hydrodynamics). Some results for $Wi = 2$ are given in Fig. 7, where we also show the analytical solution for the harmonic dimer and the results for longer tethered chains. When a hard wall is present, the numerical results show that the position of the peak in the CCF shifts to smaller times and reduces in height. For the non-linear springs, the position of the peak moves to smaller times as Wi increases, exactly as we observe for the tethered chains. The height of the peak is several times larger for a dimer than for a chain with $N \gg 1$ beads, which is not unexpected.

Even after including non-linearity and the hard wall, the dimer model fails to reproduce the smaller but still substantial negative peak at $t < 0$ that we observe in the CCFs for the longer tethered chains at small Wi. An analytical calculation for a harmonic chain tethered

to a point and subjected to shear flow might reproduce that feature as well. We can mimic such a peak by constructing an artificial CCF,

$$\hat{C}_{xy}(t) = C_{xy}(t) - \alpha C_{xy}(-t), \tag{A2}$$

where $0 < \alpha < 1$ controls the depth of the negative peak, and C_{xy} is the analytical CCF for the harmonic dimer . As illustrated in Fig. 7, such an empirical fit matches the numerical results quite well. The Fourier transform of Eq. (A2) gives an empirical PSD of the form

$$\hat{S}(2\pi\nu = \Omega/\tau) \sim Wi \frac{\sqrt{(1+\alpha^2)(1+\Omega^2) - 2\alpha(1-\Omega^2)}}{1 + 2\Omega^2 + \Omega^4},$$

which for $\alpha > 1/3$ exhibits a wide maximum at frequencies $\Omega = 2\pi\tau/T \sim 0.5$, i.e., at a period $T \sim 10\tau$. As illustrated in Fig. 7, the maximum in this PSD is very reminiscent of the "peaks" in the PSD observed in Refs.[14,15,18], where they were attributed to the existence of a periodic motion with period of about 10τ. The analytical shape of the PSD only involves τ as a relevant timescale, and the cross-correlation function has an exponential decay at large times $\sim \exp(-t/\tau)$, just like the autocorrelation function for the end-to-end vector used to define relaxation times. Such an exponential decay is inconsistent with periodic motion, but is consistent with some recent theoretical models that suggest similar correlations for a free chain in shear flow[19,20]. In summary, as seen from this simple analytical example of a dimer in a flow, a maximum in the PSD does not imply any periodic motion and the claim of an existence of a new physical timescale other than the internal relaxation time of the polymer is not justified.

---

* Electronic address: depablo@engr.wisc.edu

[1] E. S. G. Shaqfeh. The dynamics of single-molecule DNA in flow. *Journal of Non-Newtonian Fluid Mechanics*, 130(1):1–28, 2005.

[2] R.B. Bird, C.F. Curtiss, R.C. Amstrong, and O. Hasager. *Dynamics of Polymer Liquids Vol. 2.* Wiley-Interscience; 2 edition, 2001.

[3] T. T. Perkins, D. E. Smith, R. G. Larson, and S. Chu. Stretching of a single tethered polymer in a uniform-flow. *Science*, 268(5207):83–87, 1995.

[4] T. T. Perkins, D. E. Smith, and S. Chu. Single polymer dynamics in an elongational flow. *Science*, 276(5321):2016–2021, 1997.

[5] D. E. Smith and S. Chu. Response of flexible polymers to a sudden elongational flow. *Science*, 281(5381):1335–1340, 1998.

[6] D. E. Smith, H. P. Babcock, and S. Chu. Single-polymer dynamics in steady shear flow. *Science*, 283(5408):1724–1727, 1999.

[7] S. Gerashchenko and V. Steinberg. Statistics of tumbling of a single polymer molecule in shear flow. *Phys. Rev. Lett.*, 96:038304, 2006.

[8] R. M. Jendrejack, E. T. Dimalanta, D. C. Schwartz, M. D. Graham, and J. J. de Pablo. DNA dynamics in a microchannel. *Phys. Rev. Lett.*, 91(3):038102, 2003.

[9] R. M. Jendrejack, D. C. Schwartz, M. D. Graham, and J. J. de Pablo. Effect of confinement on DNA dynamics in microfluidic devices. *J. Chem. Phys.*, 119(2):1165–1173, 2003.

[10] S. T. Milner. Polymer brushes. *Science*, 251(4996):905–914, 1991.

[11] George Fytas, Spiros H. Anastasiadis, Rachid Seghrouchni, Dimitris Vlassopoulos, Junbai Li, Bradford J. Factor, Wolfgang Theobald, and Chris Toprakcioglu. Probing collective motions of terminally anchored polymers. *Science*, 274(5295):2041–2044, 1996.

[12] P. S. Doyle, B. Ladoux, and J. L. Viovy. Dynamics of a tethered polymer in shear flow. *Phys. Rev. Lett.*, 84(20):4769–4772, 2000.

[13] A. Puliafitoa and K. Turitsyn. Numerical study of polymer tumbling in linear shear flows. *Physica D: Nonlinear Phenomena*, 211(1-2):9–22, 2005.

[14] C. M. Schroeder, R. E. Teixeira, E. S. G. Shaqfeh, and S. Chu. Characteristic periodic motion of polymers in shear flow. *Phys. Rev. Lett.*, 95(1):018301, 2005.

[15] R. Delgado-Buscalioni. Cyclic motion of a grafted polymer under shear flow. *Phys. Rev. Lett*, 96(8):088303, 2006.

[16] Y. Gratton and G. W. Slater. Molecular dynamics study of tethered polymers in shear flow. *European Physical Journal E*, 17(4):455–465, 2005.

[17] A. Donev, A. L. Garcia, and B. J. Alder. Stochastic Event-Driven Molecular Dynamics. *J. Comp. Phys.*, 227(4):2644–2665, 2008.

[18] R. Delgado-Buscalioni. Dynamics of a Single Tethered Polymer under Shear Flow. *AIP Conference Proceedings*, 913(1):114–120, 2007.

[19] D. Das and S. Sabhapandit. Accurate Statistics of a Flexible Polymer Chain in Shear Flow. *Phys. Rev. Lett.*, 101(18):188301, 2008.

[20] R. G. Winkler. Semiflexible Polymers in Shear Flow. *Phys. Rev. Lett.*, 97(12):128301, 2006.

[21] L. G. Leal and E. J. Hinch. The effect of weak Brownian rotations on particles in shear flow. *J. Fluid Mech.*, 46(04):685–703, 1971.

[22] R. M. Jendrejack, J. J. de Pablo, and M. D. Graham. Stochastic simulations of DNA in flow: Dynamics and the effects of hydrodynamic interactions. *J. Chem. Phys.*, 116(17):7752–7759, 2002.

[23] P. Ahlrichs and B. Duenweg. Simulation of a single polymer chain in solution by combining lattice Boltzmann and molecular dynamics. *J. Chem. Phys.*, 111:8225, 1999.

[24] B. Duenweg and A. J. C. Ladd. Lattice Boltzmann simulations of soft matter systems. *ArXiv e-prints*, 803, 2008.

[25] R. M. Jendrejack, M. D. Graham, and J. J. de Pablo. Hydrodynamic interactions in long chain polymers: Application of the chebyshev polynomial approximation in stochastic simulations. *J. Chem. Phys.*, 113(7):2894–2900, 2000.

[26] A. Sierou and J. F. Brady. Accelerated Stokesian Dynamics simulations. *J. Fluid Mech.*, 448:115–146, 2001.

[27] J. P. Hernandez-Ortiz, J. J. de Pablo, and M. D. Graham. Fast Computation of Many-Particle Hydrodynamic and Electrostatic Interactions in a Confined Geometry. *Phys. Rev. Lett.*, 98(14):140602, 2007.

[28] J. N. Roux. Brownian particles at different times scales: a new derivation of the Smoluchowski equation. *Phys. A*, 188:526–552, 1992.

[29] J. P. Hernandez-Ortiz, H. Ma, J. J. de Pablo, and M. D. Graham. Concentration distributions during flow of confined flowing polymer solutions at finite concentration: slit and grooved channel. *Korea-Australia Rheology Journal*, 20(3):143–152, 2008.

[30] N. Sharma and N. A. Patankar. Direct numerical simulation of the Brownian motion of particles by using fluctuating hydrodynamic equations. *J. Comput. Phys.*, 201:466–486, 2004.

[31] D. Trebotich, G. H. Miller, P. Colella, D. T. Graves, D. F. Martin, and P. O. Schwartz. A Tightly Coupled Particle-Fluid Model for DNA-Laden Flows in Complex Microscale Geometries. *Comp. Fluid Solid Mech.*, pages 1018–1022, 2005.

[32] P. J. Atzberger, P. R. Kramer, and C. S. Peskin. A stochastic immersed boundary method for fluid-structure dynamics at microscopic length scales. *J. Comp. Phys.*, 224:1255–1292, 2007.

[33] O. B. Usta, A. J. C. Ladd, and J. E. Butler. Lattice-Boltzmann simulations of the dynamics of polymer solutions in periodic and confined geometries. *J. Chem. Phys.*, 122(9):094902, 2005.

[34] B. M. Boghosian, P. J. Love, P. V. Coveney, I. V. Karlin, S. Succi, and J. Yepez. Galilean-invariant lattice-Boltzmann models with H theorem. *Phys. Rev. E*, 68(2):025103, 2003.

[35] Y.-L. Chen, H. Ma, M. D. Graham, and J. J. de Pablo. Modeling DNA in Confinement: A Comparison between the Brownian Dynamics and Lattice Boltzmann Method. *Macromolecules*, 40(16):5978–5984, 2007.

[36] G. De Fabritiis, M. Serrano, R. Delgado-Buscalioni, and P. V. Coveney. Fluctuating hydrodynamic modeling of fluids at the nanoscale. *Phys. Rev. E*, 75(2):026307, 2007.

[37] J. B. Bell, A. Garcia, and S. A. Williams. Numerical Methods for the Stochastic Landau-Lifshitz Navier-Stokes Equations. *Phys. Rev. E*, 76:016708, 2007.

[38] R. Adhikari, K. Stratford, M. E. Cates, and A. J. Wagner. Fluctuating Lattice Boltzmann. *Europhysics Letters*, 71:473–479, 2005.

[39] P. R. Kramer, C. S. Peskin, and P. J. Atzberger. On the foundations of the stochastic immersed boundary method. *Computer Methods in Applied Mechanics and Engineering*, 197(25-28):2232–2249, 2008.

[40] G. Giupponi, G. De Fabritiis, and P. V. Coveney. Hybrid method coupling fluctuating hydrodynamics and molecular dynamics for the simulation of macromolecules. *J. Chem. Phys.*, 126(15):154903, 2007.

[41] S. H. Lee and R. Kapral. Mesoscopic description of solvent effects on polymer dynamics. *J. Chem. Phys.*, 124(21):214901, 2006.

[42] N. Kikuchi, J. F. Ryder, C. M. Pooley, and J. M. Yeomans. Kinetics of the polymer collapse transition: The role of hydrodynamics. *Phys. Rev. E*, 71(6):061804, 2005.

[43] K. Mussawisade, M. Ripoll, R. G. Winkler, and G. Gompper. Dynamics of polymers in a particle-based mesoscopic solvent. *J. Chem. Phys.*, 123(14):144905, 2005.

[44] F. Xijunand N. Phan-Thien, S. Chen, X. Wu, and T. Y. Ng. Simulating flow of DNA suspension using dissipative particle dynamics. *Physics of Fluids*, 18(6):063102, 2006.

[45] A. Donev, A. L. Garcia, and B. J. Alder. Stochastic Hard-Sphere Dynamics for Hydrodynamics of Non-Ideal Fluids. *Phys. Rev. Lett*, 101:075902, 2008.

[46] S. A. Williams, J. B. Bell, and A. L. Garcia. Algorithm Refinement for Fluctuating Hydrodynamics. *SIAM Multiscale Modeling and Simulation*, 6:1256–1280, 2008.

[47] R. Delgado-Buscalioni and G. De Fabritiis. Embedding molecular dynamics within fluctuating hydrodynamics in multiscale simulations of liquids. *Phys. Rev. E*, 76(3):036709, 2007.

[48] H.C. Öttinger. *Stochastic Processes in Polymeric Fluids: Tools and Examples for Developing Simulation Algorithms*. Springer, 1995.

[49] Eric R. Dufresne, Todd M. Squires, Michael P. Brenner, and David G. Grier. Hydrodynamic coupling of two brownian spheres to a planar surface. *Phys. Rev. Lett.*, 85:3317 – 3320, 2000.

[50] J.R. Blake. A note on the image system for a stokeslet in a no-slip boundary. *Proc. Camb. Philos. Soc.*, 70:303–310, 1971.

[51] R. M. Jendrejack, D. C. Schwartz, J. J. de Pablo, and M. D. Graham. Shear-induced migration in flowing polymer solutions: Simulation of long-chain deoxyribose nucleic acid in microchannels. *J. Chem. Phys.*, 120(5):2513–2529, 2004.

[52] U. S. Agarwal, A. Dutta, and R. A. Mashelkar. Effect of flexibility on the shear-induced migration of short-chain polymers in parabolic channel flow. *J. Fluid Mech.*, 557:297–306, 2006.

[53] Y.-L. Chen, M. D. Graham, K. Jo, D. C. Schwartz, and J. J. de Pablo. DNA Molecules in Microfluidic Oscillatory Flow. *Macromolecules*, 38:6680–6687, 2005.

[54] O.B. Usta, A.J.C. Ladd, , and J.E. Butler. Lattice-Boltzmann simulations of the dynamics of polymer solutions in periodic and confined geometries. *J. Chem. Phys.*, 122:094902, 2005.

[55] F. J. Alexander and A. L. Garcia. The Direct Simulation Monte Carlo Method. *Computers in Physics*, 11(6):588–593, 1997.

[56] S. W. Smith, C. K. Hall, and B. D. Freeman. Molecular Dynamics for Polymeric Fluids Using Discontinuous Potentials. *J. Comp. Phys.*, 134(1):16–30, 1997.

[57] S. Peng, F. Ding, B. Urbanc, S. V. Buldyrev, L. Cruz, H. E. Stanley, and N. V. Dokholyan. Discrete molecular dynamics simulations of peptide aggregation. *Phys. Rev. E*, 69(4):041908, 2004.

[58] H. D. Nguyen and C. K. Hall. Molecular Dynamics Simulations of Fibril Formation by Random Coil Peptides. *Proc. Natl. Acad. Sci.*, USA 101:16180, 2004.

[59] S. B. Opps, J. M. Polson, and N. A. Risk. Discontinuous molecular dynamics simulation study of polymer collapse. *J. Chem. Phys.*, 125(19):194904, 2006.

[60] C. Aust, M. Kroger, and S. Hess. Structure and dynamics of dilute polymer solutions under shear flow via nonequilibrium molecular dynamics. *Macromolecules*, 32(17):5660–5672, 1999.

[61] M. Ripoll, K. Mussawisade, R. G. Winkler, and G. Gompper. Low-Reynolds-number hydrodynamics of complex fluids by multi-particle-collision dynamics. *Europhys. Lett.*, 68(1):106, 2004.

[62] B. J. Alder and T. E. Wainwright. Studies in molecular dynamics. I. General method. *J. Chem. Phys.*, 31:459–466, 1959.

[63] A. Donev, S. Torquato, and F. H. Stillinger. Neighbor List Collision-Driven Molecular Dynamics Simulation for Nonspherical Particles: I. Algorithmic Details II. Applications to Ellipses and Ellipsoids. *J. Comp. Phys.*, 202(2):737–764, 765–793, 2005.

Figure Captions

1 Snapshots taken from a simulation run with $Wi = 5$ to show tethered DNA dynamics. The beads are labeled from 1 to 11 as shown. Cyclic motion mechanism proposed by Doyle *et al.* is composed of four stages: 1) (Re)coiling; 2) initiating; 3) stretching; 4) rotating[12]

2 Probability distribution of the end bead of the tethered DNA molecule in a dimensionless $x - z$ plane at $Wi = 0$ and $Wi = 2$. The visible differences can likely be attributed to the differences in the boundary conditions between the different methods, as well as the different elasticity of the chains. (Left) Brownian dynamics. (Middle) Stochastic Event-Driven Molecular Dynamics. (Right) Lattice Boltzmann Method.

3 Dependence of the dimensionless relaxation time $\tau(Wi)/\tau(Wi = 0)$ of the tethered chain along the three coordinate axes as a function of dimensionless flow rate Wi. The inset shows the ratios of the different relaxation times as a function of Wi.

4 (a) Normalized cross-correlation functions (CCF) $C_{zx}(t)$ of the end bead's coordinates in flow direction z and gradient direction x as a function of non-dimensional time, at various Wi for $N_s = 10$. The inset shows longer time lags. (b) Power spectral density (PSD) $S_{zx}(\nu)$ of the end bead's coordinates as a function of non-dimensional frequency. The results are averaged over 30 runs for a total simulation time is $10^3\tau$, and $10^4\tau$ for $Wi = 5$.

5 (a). CCFs of end beads' coordinates at $Wi = 2$ for a chain with $N_s = 10$ and simulation time is 1000 τ. The number in the legend is the bead label as shown in Fig. 1. The inset shows the CCFs for x coordinates of different beads to study the correlation of the dynamics between different beads (similar results are obtained for the y axes). (b) CCFs of end bead as function of chain length at $Wi = 5$. The number in the legend is the number of springs N_s in the chain. The inset shows longer time lags.

6 Comparison of the cross-correlation function $C_{zx}(t)$ at $Wi = 2$ among the three different methods: Brownian Dynamics (30 runs about $\sim 1000\tau$ long), Lattice-Boltzmann (run is $\sim 600\tau$ long), and Stochastic Event-Driven Molecular Dynamics (10 runs about $\sim 1000\tau$ long).

7 The left panel shows the cross-correlation function for a dimer (dumbbell) tethered to a hard wall and subjected to shear flow, for a harmonic, FENE and a worm-like spring. We also show a *rescaled* form of the analytical solution for a harmonic dimer in shear flow (without a hard wall). The height of the peak diminishes by a factor of about 2 when a hard wall is present, so we have rescaled the analytical solution for the harmonic dumbbell accordingly. The position of the peak shifts to smaller times when a hard wall is present as well, and we have thus rescaled the time for the analytical solution. The CCF for a wormlike chain of $N = 20$ beads, as obtained from Brownian Dynamics simulations, is also shown for qualitative comparison after *scaling* by a factor of 3 to bring its height in agreement with the dimer case. We also show an empirical fit to the Brownian Dynamics simulations of the form proposed in Eq. (A2), for which the PSD can be analytically calculated and shows a maximum at period $T \sim 10\tau$, depending on the value of the tunable parameter α, as illustrated in the right panel.

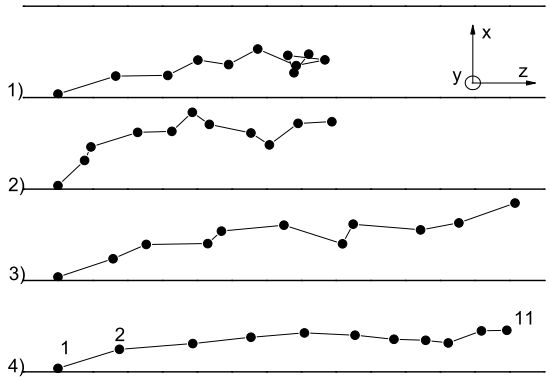

Figure 1

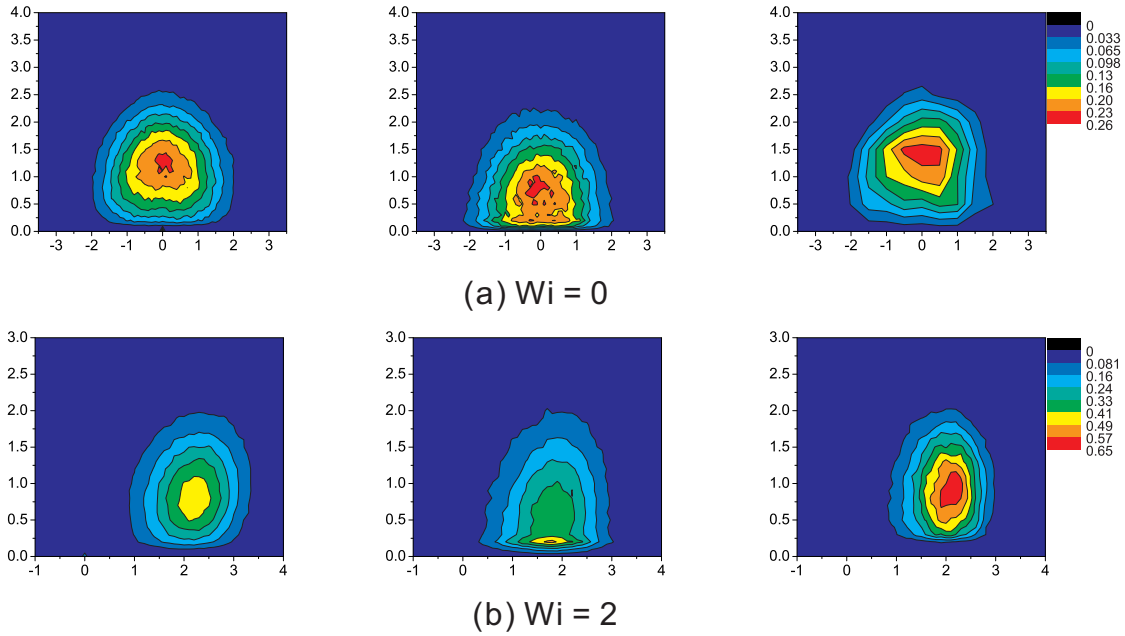
0
0.033
0.065
0.098
0.13
0.16
0.20
0.23
0.26
(a) Wi = 0
0
0.081
0.16
0.24
0.33
0.41
0.49
0.57
0.65
(b) Wi = 2

Figure 2

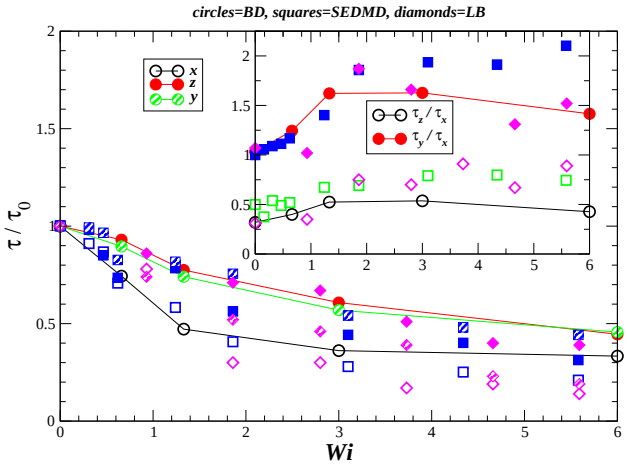

Figure 3

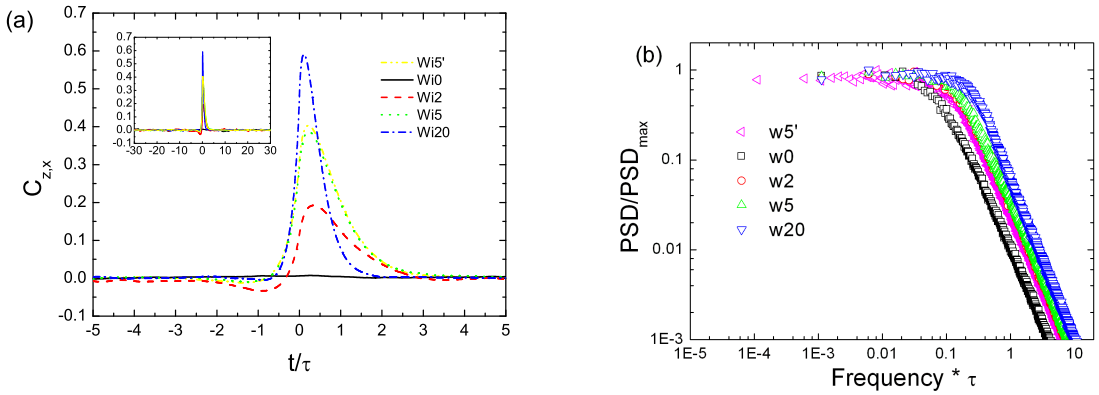
(a)
$C_{z,x}$
t/τ
Wi5'
Wi0
Wi2
Wi5
Wi20
(b)
PSD/PSD$_{max}$
Frequency * τ
w5'
w0
w2
w5
w20

Figure 4

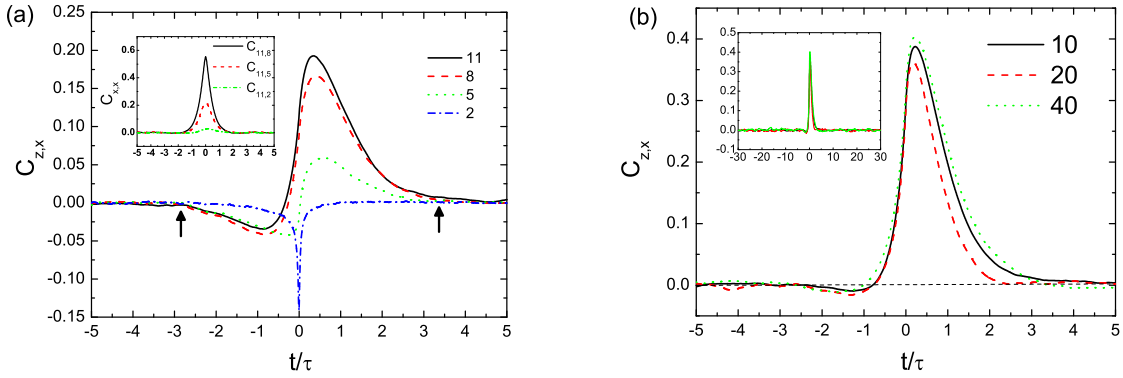

Figure 5

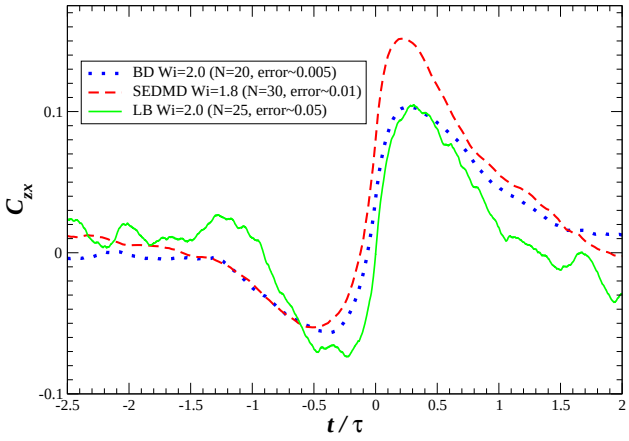
BD Wi=2.0 (N=20, error~0.005)
SEDMD Wi=1.8 (N=30, error~0.01)
LB Wi=2.0 (N=25, error~0.05)
C_{zx}
0.1
0
-0.1
-2.5
-2
-1.5
-1
-0.5
0
0.5
1
1.5
2
t / τ

Figure 6

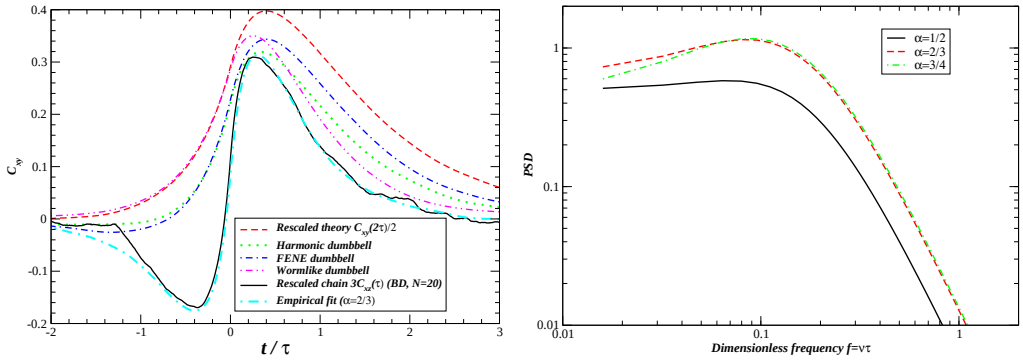
0.4
0.3
0.2
0.1
0
-0.1
-0.2
-2
-1
0
1
2
3
C_{xy}
t / τ
Rescaled theory $C_{xy}(2\tau)/2$
Harmonic dumbbell
FENE dumbbell
Wormlike dumbbell
Rescaled chain $3C_{xy}(\tau)$ (BD, N=20)
Empirical fit (α=2/3)
1
0.1
0.01
0.01
0.1
1
PSD
Dimensionless frequency f=ντ
α=1/2
α=2/3
α=3/4

Figure 7